Chemical Vapor Deposition

Deutsche Ausgabe: DOI: 10.1002/ange.201604445
Internationale Ausgabe: DOI: 10.1002/anie.201604445

Solid–Vapor Reaction Growth of Transition-Metal Dichalcogenide Monolayers

Bo Li[+], Yongji Gong[+], Zhili Hu, Gustavo Brunetto, Yingchao Yang, Gonglan Ye, Zhuhua Zhang, Sidong Lei, Zehua Jin, Elisabeth Bianco, Xiang Zhang, Weipeng Wang, Jun Lou, Douglas S. Galvão, Ming Tang, Boris I. Yakobson, Robert Vajtai, and Pulickel M. Ajayan**

Abstract: *Two-dimensional (2D) layered semiconducting transition-metal dichalcogenides (TMDCs) are promising candidates for next-generation ultrathin, flexible, and transparent electronics. Chemical vapor deposition (CVD) is a promising method for their controllable, scalable synthesis but the growth mechanism is poorly understood. Herein, we present systematic studies to understand the CVD growth mechanism of monolayer $MoSe_2$, showing reaction pathways for growth from solid and vapor precursors. Examination of metastable nanoparticles deposited on the substrate during growth shows intermediate growth stages and conversion of non-stoichiometric nanoparticles into stoichiometric 2D $MoSe_2$ monolayers. The growth steps involve the evaporation and reduction of MoO_3 solid precursors to sub-oxides and stepwise reactions with Se vapor to finally form $MoSe_2$. The experimental results and proposed model were corroborated by ab initio Car–Parrinello molecular dynamics studies.*

The rise of layered two-dimensional (2D) materials has initiated a new era in materials innovation.[1] Semiconducting transition-metal dichalcogenides (TMDCs) have emerged as promising candidates for next-generation ultrathin, flexible, and transparent electronics.[1g–k,2] Recent progress in chemical vapor deposition (CVD) has shown that high-quality single crystals and wafer-scale continuous films of controlled thickness can be obtained, driving the development of TMDCs for these applications.[1j,2d,e,3] Whereas some aspects (e.g., crystal and film size, defects, number of layers) can be controlled,[2d,3a] the development of CVD methods for the synthesis of TMDCs has reached a bottleneck, and further progress is unlikely if the growth mechanism is not fully understood.

Diverse growth methods and mechanisms have been described for various nanomaterials, including vapor–liquid–solid (VLS) processes for nanowire synthesis[4] and vapor-phase reactions for TMDC nanoparticles.[5] The CVD method is one of the most promising techniques for synthesizing large-scale 2D materials,[1d,e,2d,3a,6] exceeding the size limitations of other methods, such as mechanical exfoliation[1a] and the catalyst-free vapor–solid (VS) syntheses (demonstrated for MoS_2, Bi_2Se_3, and Bi_2Te_3).[7] The CVD growth mechanism of graphene has been investigated in detail, and is known to be substrate-dependent.[8] On Ni substrates, the growth is generally believed to be the precipitation of dissolved carbon, whereas on Cu substrates, it is a catalytic growth process.[1d,e] The CVD growth of TMDCs, however, involves multiple reactants and products, and is significantly more complicated than graphene growth. Identification of the byproducts formed during TMDC growth is also challenging because post-growth analysis is often prohibited by the formation of contaminants during the cooling process. Therefore, despite tremendous research efforts to grow various TMDC materials[1i–k,2d,e] and heterogeneous analogues,[9] the CVD growth process of TMDCs is currently not well understood.

Herein, we analyzed the CVD growth mechanism of 2D $MoSe_2$. Samples were quenched halfway through a typical CVD growth process and compared to those that were slowly cooled to completion. The intermediate phases in the quenched samples were then analyzed. Based on the co-existence of $MoSe_2$, aligned nanoparticles (APs) at the crystalline edges of $MoSe_2$, and randomly distributed nanoparticles (RPs), as well as evidence of an in-plane "feedstock" and $MoSe_2$ nucleation from the RPs, we developed a three-step growth model and proposed chemical reactions for each step, which were corroborated by molecular dynamics simulations. The first model of the CVD growth process of TMDCs has thus been developed. Furthermore, the growth of $MoSe_2$ was shown to be a reversible reaction, where the $MoSe_2$ edges recede during the slow cooling process.

As shown in Figure 1 a, a chip of Si/SiO_2 wafer was placed on top of a crucible preloaded with MoO_3 powder in the center of a tube furnace. Se powder was placed upstream of the wafer, and Ar/H_2 (85/15 %) was used as the carrier gas. The furnace was heated to 750 °C from room temperature at

[*] Dr. B. Li,[+] Dr. Y. Gong,[+] Dr. Z. Hu, Dr. G. Brunetto, Dr. Y. Yang, G. Ye, Dr. Z. Zhang, Dr. S. Lei, Z. Jin, X. Zhang, Dr. W. Wang, Prof. J. Lou, Prof. M. Tang, Prof. B. I. Yakobson, Dr. R. Vajtai, Prof. P. M. Ajayan
Department of Materials Science & NanoEngineering
Rice University, Houston, TX 77005 (USA)
E-mail: robert.vajtai@rice.edu
ajayan@rice.edu
Dr. Y. Gong,[+] E. Bianco, Prof. P. M. Ajayan
Department of Chemistry, Rice University
Houston, TX 77005 (USA)
Dr. G. Brunetto, Prof. D. S. Galvão
Instituto de Fisica "Gleb Wataghin"
Universidade Estadual de Campinas
Unicamp, CP 6165, 13083-970 Campinas, Sao Paulo (Brazil)
Dr. Z. Zhang
State Key Laboratory of Mechanics and Control of Mechanical Structures
Nanjing University of Aeronautics and Astronautics
Nanjing 210016 (China)
[+] These authors contributed equally to this work.
Supporting information and the ORCID identification number for an author of this article can be found under http://dx.doi.org/10.1002/anie.201604445.

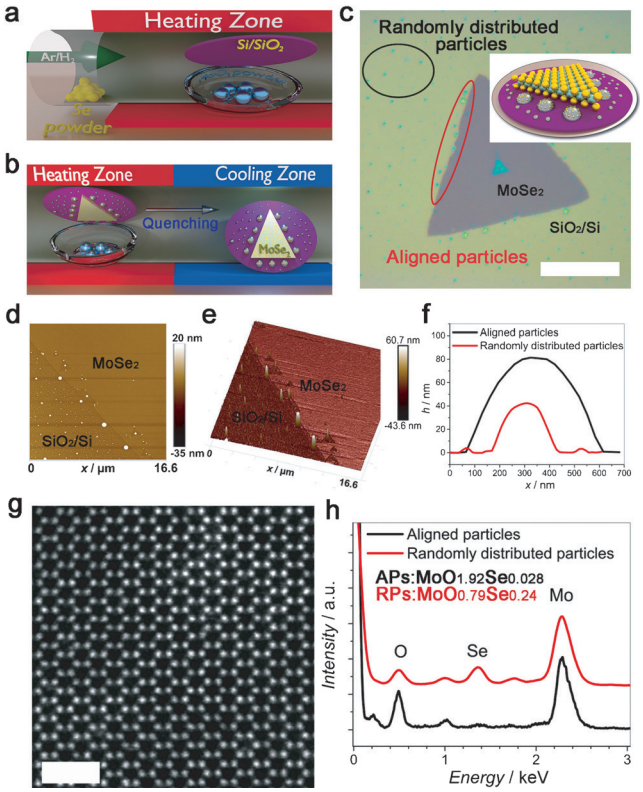

Figure 1. a) The growth process and b) the quenching process. c) Optical image of $MoSe_2$ grown on a SiO_2/Si substrate together with APs along the edge of $MoSe_2$ and RPs. Inset: Schematic representation of the quenched substrate. d, e) The AFM topology of the $MoSe_2$ edge, 2D (d) and 3D (e) views. f) The line profiles of APs near the edge and RPs. The height of the APs was about 80 nm with a diameter of approximately 500 nm. The heights of the RPs are in the range of several nanometers to tenths of nanometers. Overall, the RPs are much smaller than the APs. g) STEM image of monolayer $MoSe_2$. h) EDX spectra of APs and RPs. The marked peaks of interest for Mo, Se, and O are located at 2.29, 1.37, and 0.51 keV, respectively, with unmarked peaks from the background of Cu (0.99 keV) and Si (1.75 keV). Scale bars: 20 μm for (c) and 1 nm for (g).

a rate of 50 °C min^{-1} and then held at 750 °C for the growth of $MoSe_2$. The quenching procedure was performed by relocating the crucible from the center of the furnace (750 °C) to room temperature (ca. 25 °C) within one second after holding at 750 °C for 10 min (Figure 1 b). For comparison, we also performed slow cooling experiments in which a constant cooling rate of 12.5 °C min^{-1} was applied after heating to 750 °C at the same rate and holding the temperature for 5 to 60 min.

After quenching the growth process at 10 min, three types of components, which were distinctly different in size, composition, and morphology, were found on the substrate. As shown in Figure 1 c, triangular-shaped single crystals of $MoSe_2$ were formed, along with APs at the crystalline edges of $MoSe_2$ and RPs found elsewhere on the substrate (see the Supporting Information, Figure S1 a–f). $MoSe_2$ gave Raman peaks at 239 cm^{-1} (A_{1g}) and 285 cm^{-1} (E'_{2g}; Figure S1 g), which is consistent with the A_{1g} and E'_{2g} peaks of single-layer $MoSe_2$,[3b,c,10] whereas both the APs and RPs showed no signature peaks (Figure S1 h, i). At the edges of the single crystals, well-ordered lines of APs are present, with a diameter of about 500 nm and a height of approximately 80 nm, as determined by atomic force microscopy (AFM; Figure 1 d–f). The RPs, which were randomly dispersed away from the crystalline edges, are much smaller and have a wider size distribution, with diameters ranging from several nanometers to as large as about 200 nm and heights from several nanometers to tens of nanometers (Figure 1 c–f; see also Figure S1). High-angle annular dark field (HAADF) scanning transmission electron microscopy (STEM; Figure 1 g) confirmed the highly crystalline nature of the $MoSe_2$ monolayer. High-resolution STEM images of the APs and RPs were unattainable as their size precluded penetration by the electron beam. Instead, selected area electron diffraction (SAED; Figure S2 b, g) and energy-dispersive X-ray spectroscopy (EDX; Figure 1 h and Figure S2 c–e, h–j) analysis were performed to determine the structure and composition of these particles. The EDX results were obtained by accumulating the mapping results of multiple particles as shown in Figure 1 h (see also Figure S2). The marked peaks of interest for Mo, Se, and O are located at 2.29, 1.37, and 0.51 keV, respectively, with unmarked peaks from the background of Cu (0.99 keV) and Si (1.75 keV). The atomic ratio of the RPs according to the mapping analysis is $MoO_{0.79}Se_{0.24}$, with the entire index normalized to the Mo content. The atomic ratio of the APs is $MoO_{1.92}Se_{0.028}$; the oxygen content is almost two while the Se content is substantially diminished. The SAED patterns indicate that both the APs and RPs are amorphous (Figure S2 b, g).

Considering the striking differences in the atomic composition and the distribution of the two types of nanoparticles, we suggest a unique growth mechanism that has never been considered for 2D layered TMDC growth. The growth of graphene and TMDC fullerene-like nanoparticles (with a similar chemical composition but a different morphology to TMDC 2D layers) is generally believed to be a vapor-phase reaction.[1d,e,5a] However, in this case, the presence of different MoO_xSe_y nanoparticles and their potential for subsequent selenization suggest that the CVD growth of $MoSe_2$ could be a solid- or liquid-phase reaction where the nanoparticles serve as a reactant. The alignment between the edge of $MoSe_2$ and the APs suggests that the APs are byproducts of the $MoSe_2$ growth. The size distribution of the RPs indicates that they are coarsening particles formed by the condensation process during the CVD growth, as shown in Figure 1 d–f (see also Figure S1). One argument might be that these two types of nanoparticles are condensed phases that are formed during the fast cooling process. However, if this is true, the two types of nanoparticles should have similar compositions and spatial distributions as the gas-phase environment near the substrate should be uniform. However, the compositions and sizes of APs and nearby RPs are different.

The proposition that the RPs are an intermediate reactant for $MoSe_2$ growth arose from the observation of multilayered $MoSe_2$ with the top layer containing a shaped domain looking like the "radioactive warning sign" (Figure 2 a). We hypothesized that the three triangular grains seen in this domain are likely to have grown from small adjacent $MoSe_2$ nuclei with

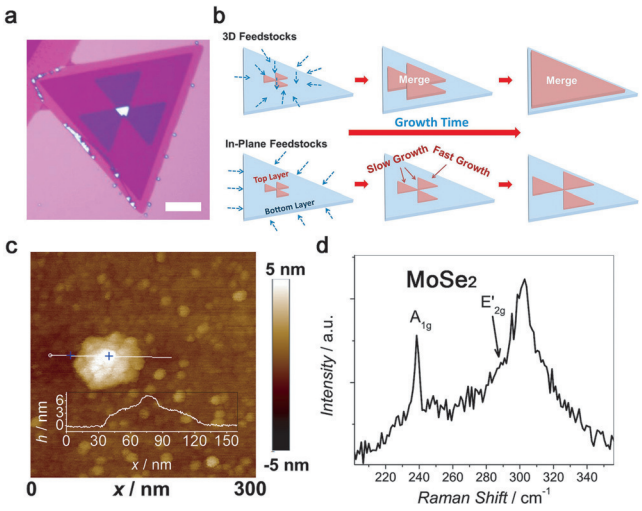

Figure 2. a) Trilayer $MoSe_2$ with a radiation-signal grain on the top layer. Scale bar: 10 μm. b) The evolvement of a small radiation-signal grain on the top of the bottom layer in different feedstock modes. In the 3D feedstock mode, the three grains will grow and merge and eventually become a large triangle. In the in-plane feedstock mode, with at least one of the necessary reactants supplied from within the plane, the differences in diffusion length will cause a faster growth at the edges close to the reactant and slower growth at the inner edges, leading to separate triangles. c) AFM image of an RP after annealing at 700 °C for 10 min with the same H_2/Ar environment, but no Se and MoO_3 sources. The hexagonally shaped nucleus was developed from an RP. Inset: Line profile of the nanoparticle along the white line in (c). d) Raman spectrum of the nucleus showing the representative $MoSe_2$ signals.

the same crystalline orientation on the top of the bottom layer. If the growth of these nuclei was isotropic, as from a three-dimensional (3D) gas-phase feedstock, they should have quickly merged and formed a single grain (schematically shown in Figure 2b, top) instead of three individual grains. However, as illustrated in Figure 2b (bottom), the observed domain morphology may arise if the domain growth relies on the in-plane (inward) diffusion of the Mo feedstock from the surrounding RPs on the substrate. Such a reactant diffusion process could cause the outer edge of the triangular grain to grow faster than the two inner edges owing to the shorter diffusion distance, and hence, it receives a larger diffusion flux. Collectively, the experimental results presented above reveal that the vapor-phase growth mechanism proposed for both graphene and TMDC nanoparticles is not valid for the growth of layered TMDCs.

Assuming that the RPs are a necessary reaction intermediate, we hypothesized that the RPs form the nuclei of the single crystals during growth. To confirm this hypothesis, a quenched sample was annealed at 700 °C under the same reducing environment (H_2/Ar) for 10 min with no supply of Se or MoO_3. The subsequent AFM image shows the formation of a hexagonal nucleus with a thickness of 6 nm (Figure 2c) that exhibited the characteristic Raman signatures of $MoSe_2$, A_{1g} at 239 cm^{-1} and E'_{2g} at 285 cm^{-1} (observed as a shoulder peak under the background peak of Si at 300 cm^{-1} in Figure 2d). This result suggests that even in RPs, which are Se-deficient (the Mo content is more than 4 times greater than that of Se), $MoSe_2$ nuclei "precipitate" from Mo-rich RPs at high temperature without further supply of Se or Mo. This experiment provides the first direct observation of the formation of $MoSe_2$ nuclei preceding single-crystal growth.

To further confirm that the RPs are a reactant in $MoSe_2$ growth, we estimated the total volume of RPs in representative regions of the AFM images based on the height profiles. Simple calculations show that the amount of Mo atoms available in the RPs in these regions is sufficient to form a ten-layer $MoSe_2$ crystal that covers the entire region. Moreover, the amount of Mo in the RPs was found to be much greater than that in $MoSe_2$ and APs combined in quenched samples (Figure S3 and S4 and Section S3). This results suggests that the RPs can indeed supply a sufficiently large amount of Mo atoms to facilitate $MoSe_2$ growth.

Given the central role of the RPs as reaction intermediates in the CVD growth of $MoSe_2$, we propose the following three-step growth model: I) reduction and evaporation of MoO_3 to a Mo suboxide (MoO_x, $0 < x < 3$), II) co-condensation of the Mo suboxide and Se into RPs, III) selenization of the RPs by the vapor-phase Se to form $MoSe_2$ and APs (Figure 3a). In step I, MoO_3 is reduced by H_2 (15 %)/Ar gas to form MoO_x and H_2O. The value of x ($x = 0.79$) was determined from the composition of the RPs. This step has been well-established by Feldman et al., and the sublimation temperature of MoO_x ($0 < x < 3$) can be as low as 650 °C, which is well below the temperature (750 °C) used in our CVD process.[5c] In step II, reduced MoO_x vapor interacts with the Se vapor phase and condenses on the wafer, forming RPs with the composition MoO_xSe_y ($x = 0.79$, $y = 0.24$). It is interesting to note that adding a small amount of Se leads to significant MoO_x condensation. The RPs are composites of reduced MoO_x and Se, not compounds with fixed stoichiometry, which was confirmed by the fact that the composition of the RPs varies from point to point (MoO_xSe_y, $0.22 < x < 1.25$, $0.13 < y < 0.5$; Figure S2c–e and Table S1). Finally, in step III, the RPs react with vapor-phase Se to form $MoSe_2$ and expel oxygen into the O-rich APs that decorate the edges of the $MoSe_2$ crystals. The reactions involved in the three-step model can be written as:

$$MoO_3 + H_2 \rightarrow MoO_x + H_2O \quad (1)$$

$$MoO_x + Se \rightarrow MoO_xSe_y \quad (2)$$

$$MoO_xSe_y + Se \rightarrow MoSe_2 + MoO_z \quad (3)$$

The proposed mechanism was supported by Car–Parrinello molecular dynamics (CPMD) simulations.[11] Our starting structural model is a single-layer $MoSe_2$ crystal, and single molecular/atomic species (Mo–O and/or Se) were added from a distance of about 5.2 Å away from the Se-terminated zigzag edge step by step (Figure 3b; both front and top views of each step are presented). This distance was determined to be far enough to prevent initial interactions between added species and the $MoSe_2$ edge but close enough to allow for interactions to occur within the simulation time. The system was allowed to evolve freely in time. As the RPs are a condensed

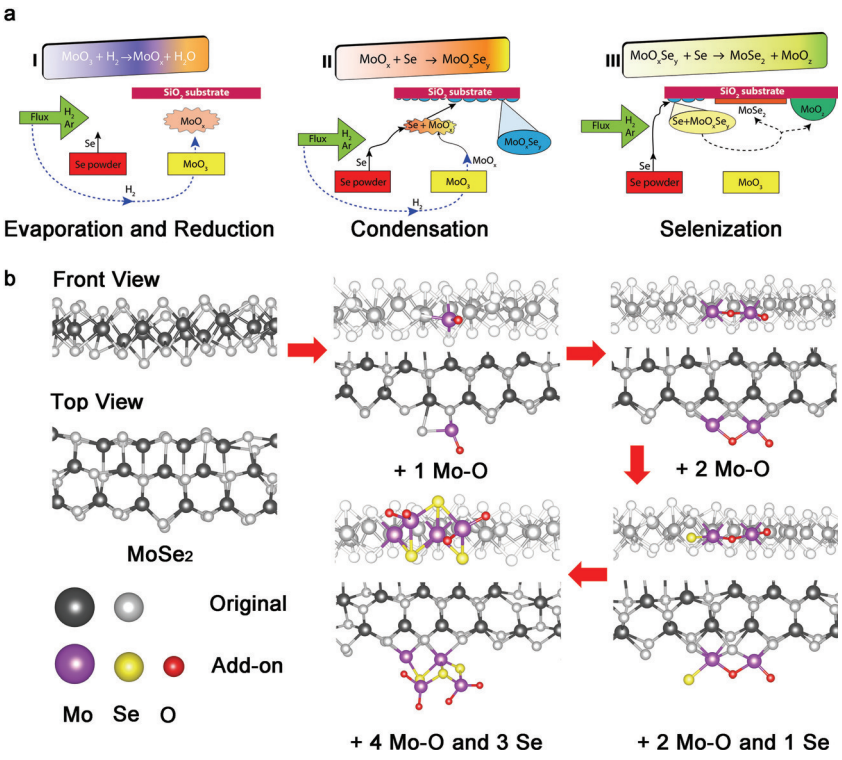

Figure 3. a) The three-step growth model: I) evaporation and reduction of MoO_3 to MoO_x, II) condensation of MoO_x by adding Se to form RPs (MoO_xSe_y, $x=0.79$, $y=0.24$) on the SiO_2/Si substrate, and III) selenization of the PRs to form $MoSe_2$ and APs (MoO_z, $z\approx2$) with a trace amount of Se. b) CPMD simulations with different numbers of Mo–O and Se units added to the original $MoSe_2$ layer step by step: 1 Mo–O, 2 Mo–O, 2 Mo–O and 1 Se, and 4 Mo–O and 3 Se. The numbers indicate the species added in each step. The original $MoSe_2$ is presented by a black-and-white stick–ball model (Mo black, Se white). The added Mo, Se, and O atoms are shown as purple, yellow, and red balls, respectively. The color contrasts of the original $MoSe_2$ were tuned down in the front views to highlight the added structures.

composite of MoO_x and Se with a Mo/O ratio of about 1, we considered Mo–O and Se as the reactants instead of the experimentally observed atomic ratio of the RPs. This allowed the analysis to be performed on a reasonable simulation timescale. No signature indicative of a Se–O bond (ca. 65 eV) was present in the XPS spectrum (Figure S5a), ruling out the possibility of Se–O being a reactant.

As time evolves, the addition of the first Mo–O species causes a local disruption (Figure 3b), resulting in the displacement of one Se atom from its initial position. However, when a second Mo–O molecule was added, the displaced Se atom migrated back to its original position together with the new Mo atom, which was then bonded to the $MoSe_2$ layer. The oxygen atoms moved outwards from the zigzag edge, and the Mo atoms were located in the same plane as the other Mo atoms initially belonging to the $MoSe_2$ sheet. Then, one Se atom was introduced in the simulation, and bonded to the exposed Mo at the crystalline edge. In the last step, a fourth Mo–O and a third Se atom were introduced. In this step, we monitored time-resolved configurations to visualize how the system assembly occurs (Figure S6 and Movie S1). It is interesting to note that as the two Mo atoms bond to the lattice of $MoSe_2$, the four oxygen atoms present in the system are pushed outwards and migrate to two "unoccupied" Mo atoms, forming two MoO_2 molecules (or a Mo_2O_4 cluster) bonded to the edge of the $MoSe_2$ crystal. Figure S6f shows the time-resolved energy evolution of the system during the reactions in Figure 3b, where the energy differences were obtained by taking the difference between the system after each reaction and the initial energy of pristine $MoSe_2$ and the four isolated Mo–O and three Se species. The system energies after each "addition" step are represented by the plateaus, and the addition of Mo–O and Se species caused the system energy to decrease substantially. The decrease in system energy suggests that the reactions of these species with the $MoSe_2$ lattice are favorable. This is consistent with the evolution of the energy in the real system, where the RPs ($MoO_{0.79}Se_{0.24}$) are not a stable intermediate and tend to decompose into the more stable $MoSe_2$ and MoO_z in the presence of vapor-phase Se.

The accumulated EDX mapping results suggest that the overall composition of the APs is close to MoO_2; however, other forms of molybdenum suboxides are also present (MoO_z, $z>1.5$; Figure S2 and Table S2). The MoO_z molecules should finally be expelled from the $MoSe_2$ edge, yielding the terminated $MoSe_2$ crystal. With the accumulation of MoO_z on the growing edge, we hypothesize that the MoO_z would eventually aggregate and evolve into a nanoscale agglomerate, exceeding a critical size where the thermal agitation would detach it from the edge of $MoSe_2$. The detached MoO_z agglomerate would initially be in the vapor phase at the growth temperature of 750 °C owing to the small size effect.[12] Owing to the requirement to reduce the overall energy, these agglomerates tend to coagulate and deposit as a condensed phase, which leads to the formation of APs as byproducts of the synthesis close to the edge of $MoSe_2$.[13] The surface of the RPs near the growth front (crystalline edge) may serve as the heterogeneous nucleation sites, which explains the presence of trace amounts of Se in the APs. This hypothesis was supported by detailed volume and composition computational analysis in comparison with the RPs (Section S3.3).

The trace amount of Se also suggests that the formation of $MoSe_2$ and the APs is faster than the timescale of Se diffusion into the APs. In fact, vapor-phase Se has the potential to diffuse into APs, as supported by a slow cooling experiment, in which the CVD growth time was again 10 min, followed by cooling at a constant rate of 12.5 °C min^{-1}. The composition of the slowly cooled APs was found to be $MoO_{2.59}Se_{0.93}$ (Figure S5d). The XPS data even suggest the formation of SeO_2 (Figure S5b). The significant increase in the oxygen (from $x=$ 0.79 to 2.59) and Se content (from $y=0.028$ to 0.93) indicates

that Se and a less-reduced MoO_x species from the vapor phase continuously deposit, changing the composition of the APs during the cooling process. This result confirms that Se is too slow to diffuse into the rapidly growing APs during the growth process. Moreover, the change in the composition of the APs during slow cooling suggests the unique advantage of the quenching technique in obtaining in situ information on the growth process.

It is also interesting to note that the reaction to form $MoSe_2$ is reversible, and a receding of the growth front and nanoparticle regrowth can be observed in the slow-cooled samples after different growth times (Figure 4 and Figure S7).

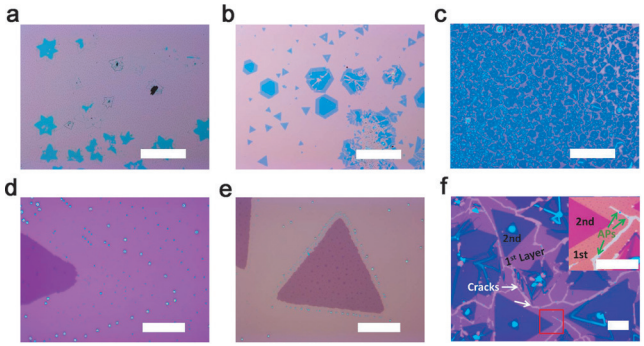

Figure 4. The degradation of $MoSe_2$ during slow cooling at a cooling rate of 12.5 °C min^{-1}. Optical images of slowly cooled samples heated to 750 °C and held at that temperature for different periods of time: a, d) 5 min, b, e) 10 min, c, f) 60 min. Scale bars: 400 μm in (a)–(c) and 20 μm in (d)–(f) and the inset.

We have demonstrated that the APs will decorate the growth front after quenching (the distance between the APs and the front ranges from 0 to about 200 nm) and can be used as markers for the original location of the $MoSe_2$ single-crystal edges. In sharp contrast, larger gaps of about 30 μm after 5 min growth and approximately 1–2 μm after 10 min growth were observed for slowly cooled samples (Figure 4 a and d, b and e). We surmise that the observed variation in gap width is correlated with the quality of the $MoSe_2$ crystals; $MoSe_2$ grown for a shorter period of time (e.g., the 5 min sample) tends to be more defective, and the edge is thus "etched" away at a higher rate during slow cooling than those grown for a longer time. This hypothesis was confirmed by a third sample with an extremely long growth time (60 min) in which the $MoSe_2$ displayed no signs of degradation (Figure 4 c and f). Here, the APs are sandwiched in the gaps between nearby crystals.

Finally, it is important to note that these nanoparticles (both APs and RPs) have also been observed in the CVD growth of other TMDC materials (such as MoS_2 and WSe_2; Figure S8), highlighting the active role of the nanoparticles in the growth process as well as in understanding the growth mechanism. Therefore, we believe that this growth model and method could provide general insight into the CVD growth of all TMDCs.

In conclusion, we have presented the first comprehensive analysis of the CVD growth mechanism of atomic-layered TMDCs. Unlike the generally accepted vapor-phase reaction mechanisms for graphene and TMDC nanoparticles, this mechanism demonstrates the important role of a metastable nanoparticle reaction intermediate ($MoO_{0.79}Se_{0.24}$), which serves as both the direct source of Mo and the nucleation site for the formation of layered $MoSe_2$. Quenching and long-time growth experiments also highlight strategies to obtain high-quality TMDCs, and suggest the reversibility and in-plane nature of the growth process. With similar phenomena observed for other layered TMDCs, we believe that this investigation will lead to further progress in improving the crystalline quality and large-area growth of these exciting 2D materials.

Acknowledgements

This work was supported in part by the Army Research Office (MURI grant W911NF-11-1-0362), and by FAME, one of six centers of STARnet, a Semiconductor Research Corporation Program sponsored by MARCO and DARPA. G.B. and D.S.G. acknowledge financial support from the Brazilian Agencies CNPq, CAPES, and FAPESP and also thank the Center for Computational Engineering and Sciences at Unicamp for financial support through the FAPESP/CEPID Grant 2013/08293-7. Z.H., Z.Z., and B.I.Y. acknowledge support from the DOE BES (Grant DE-SC0012547). M.T. acknowledges support from the DOE Office of Basic Energy Sciences Physical Behavior of Materials Program (DE-SC0014435). Y.Y. and J.L. acknowledge support from the Welch Foundation (Grant C-1716). Z.J. and J.L. are grateful for support through the AFOSR Grant FA9550-14-1-0268. We also thank Dr. Wu Zhou for providing STEM images and Dr. Qinghong Yuan and Dr. Xiaolong Zou (Rice University) as well as Prof. Chuanhong Jin and Prof. Mingsheng Xu (Zhejiang University) for helpful discussions.

Keywords: chemical vapor deposition · growth mechanisms · molybdenum diselenide · monolayers · transition-metal dichalcogenide

How to cite: *Angew. Chem. Int. Ed.* **2016**, *55*, 10656–10661
Angew. Chem. **2016**, *128*, 10814–10819

[1] a) K. S. Novoselov, A. K. Geim, S. Morozov, D. Jiang, Y. Zhang, S. Dubonos, I. Grigorieva, A. Firsov, *Science* **2004**, *306*, 666–669; b) Y. Zhang, Y.-W. Tan, H. L. Stormer, P. Kim, *Nature* **2005**, *438*, 201–204; c) A. K. Geim, K. S. Novoselov, *Nat. Mater.* **2007**, *6*, 183–191; d) K. S. Kim, Y. Zhao, H. Jang, S. Y. Lee, J. M. Kim, K. S. Kim, J.-H. Ahn, P. Kim, J.-Y. Choi, B. H. Hong, *Nature* **2009**, *457*, 706–710; e) X. Li, W. Cai, J. An, S. Kim, J. Nah, D. Yang, R. Piner, A. Velamakanni, I. Jung, E. Tutuc, *Science* **2009**, *324*, 1312–1314; f) G.-H. Lee, R. C. Cooper, S. J. An, S. Lee, A. van der Zande, N. Petrone, A. G. Hammerberg, C. Lee, B. Crawford, W. Oliver, *Science* **2013**, *340*, 1073–1076; g) K. F. Mak, C. Lee, J. Hone, J. Shan, T. F. Heinz, *Phys. Rev. Lett.* **2010**, *105*, 136805; h) B. Radisavljevic, A. Radenovic, J. Brivio, V. Giacometti, A. Kis, *Nat. Nanotechnol.* **2011**, *6*, 147–150; i) Q. H. Wang, K. Kalantar-Zadeh, A. Kis, J. N. Coleman, M. S. Strano, *Nat. Nanotechnol.* **2012**, *7*, 699–712; j) S. Najmaei, Z. Liu, W. Zhou, X. L. Zou, G. Shi, S. D. Lei, B. I. Yakobson, J. C. Idrobo, P. M. Ajayan, J. Lou, *Nat. Mater.* **2013**, *12*, 754–759; k) A. M.

van der Zande, P. Y. Huang, D. A. Chenet, T. C. Berkelbach, Y. You, G.-H. Lee, T. F. Heinz, D. R. Reichman, D. A. Muller, J. C. Hone, *Nat. Mater.* **2013**, *12*, 554 – 561.

[2] a) B. Radisavljevic, A. Kis, *Nat. Mater.* **2013**, *12*, 815 – 820; b) S. Wu, S. Buckley, J. R. Schaibley, L. Feng, J. Yan, D. G. Mandrus, F. Hatami, W. Yao, J. Vučković, A. Majumdar, *Nature* **2015**, *520*, 69 – 72; c) Y.-M. He, G. Clark, J. R. Schaibley, Y. He, M.-C. Chen, Y.-J. Wei, X. Ding, Q. Zhang, W. Yao, X. Xu, *Nat. Nanotechnol.* **2015**, *10*, 497; d) K. Kang, S. Xie, L. Huang, Y. Han, P. Y. Huang, K. F. Mak, C.-J. Kim, D. Muller, J. Park, *Nature* **2015**, *520*, 656 – 660; e) H. Zhou, C. Wang, J. C. Shaw, R. Cheng, Y. Chen, X. Huang, Y. Liu, N. O. Weiss, Z. Lin, Y. Huang, *Nano Lett.* **2015**, *15*, 709 – 713.

[3] a) Y. J. Gong, G. Ye, S. D. Lei, S. Gang, Y. He, J. Lin, X. Zhang, R. Vajtai, S. T. Pantelides, W. Zhou, B. Li, P. M. Ajayan, *Adv. Funct. Mater.* **2016**, *26*, 2009 – 2015; b) X. Wang, Y. Gong, G. Shi, W. L. Chow, K. Keyshar, G. Ye, R. Vajtai, J. Lou, Z. Liu, E. Ringe, *ACS Nano* **2014**, *8*, 5125 – 5131; c) J. C. Shaw, H. Zhou, Y. Chen, N. O. Weiss, Y. Liu, Y. Huang, X. Duan, *Nano Res.* **2014**, *7*, 511 – 517.

[4] a) H.-J. Choi, *Semiconductor Nanostructures for Optoelectronic Devices*, Springer, **2012**, pp. 1 – 36; b) Y. Wu, P. Yang, *J. Am. Chem. Soc.* **2001**, *123*, 3165 – 3166; c) C. M. Lieber, *Solid State Commun.* **1998**, *107*, 607 – 616.

[5] a) A. Zak, Y. Feldman, V. Alperovich, R. Rosentsveig, R. Tenne, *J. Am. Chem. Soc.* **2000**, *122*, 11108 – 11116; b) Y. Feldman, G. Frey, M. Homyonfer, V. Lyakhovitskaya, L. Margulis, H. Cohen, G. Hodes, J. Hutchison, R. Tenne, *J. Am. Chem. Soc.* **1996**, *118*, 5362 – 5367; c) Y. Feldman, E. Wasserman, D. Srolovitz, R. Tenne, *Science* **1995**, *267*, 222 – 225.

[6] a) J.-H. Lee, E. K. Lee, W.-J. Joo, Y. Jang, B.-S. Kim, J. Y. Lim, S.-H. Choi, S. J. Ahn, J. R. Ahn, M.-H. Park, *Science* **2014**, *344*, 286 – 289; b) L. Gao, G.-X. Ni, Y. Liu, B. Liu, A. H. C. Neto, K. P. Loh, *Nature* **2014**, *505*, 190 – 194.

[7] a) D. Kong, W. Dang, J. J. Cha, H. Li, S. Meister, H. Peng, Z. Liu, Y. Cui, *Nano Lett.* **2010**, *10*, 2245 – 2250; b) S. Wu, C. Huang, G. Aivazian, J. S. Ross, D. H. Cobden, X. Xu, *ACS Nano* **2013**, *7*, 2768 – 2772.

[8] Y. Zhang, L. Zhang, C. Zhou, *Acc. Chem. Res.* **2013**, *46*, 2329 – 2339.

[9] a) Y. Gong, S. Lei, G. Ye, B. Li, Y. He, K. Keyshar, X. Zhang, Q. Wang, J. Lou, Z. Liu, *Nano Lett.* **2015**, *15*, 6135 – 6141; b) Y. Gong, J. Lin, X. Wang, G. Shi, S. Lei, Z. Lin, X. Zou, G. Ye, R. Vajtai, B. I. Yakobson, *Nat. Mater.* **2014**, *13*, 1135 – 1142; c) X. Duan, C. Wang, J. C. Shaw, R. Cheng, Y. Chen, H. Li, X. Wu, Y. Tang, Q. Zhang, A. Pan, *Nat. Nanotechnol.* **2014**, *9*, 1024; d) C. Huang, S. Wu, A. M. Sanchez, J. J. Peters, R. Beanland, J. S. Ross, P. Rivera, W. Yao, D. H. Cobden, X. Xu, *Nat. Mater.* **2014**, *13*, 1096 – 1101; e) M.-Y. Li, Y. Shi, C.-C. Cheng, L.-S. Lu, Y.-C. Lin, H.-L. Tang, M.-L. Tsai, C.-W. Chu, K.-H. Wei, J.-H. He, *Science* **2015**, *349*, 524 – 528.

[10] P. Tonndorf, R. Schmidt, P. Böttger, X. Zhang, J. Börner, A. Liebig, M. Albrecht, C. Kloc, O. Gordan, D. R. Zahn, *Opt. Express* **2013**, *21*, 4908 – 4916.

[11] a) T. D. Kühne, M. Krack, F. R. Mohamed, M. Parrinello, *Phys. Rev. Lett.* **2007**, *98*, 066401; b) R. Car, M. Parrinello, *Phys. Rev. Lett.* **1985**, *55*, 2471.

[12] E. Roduner, *Chem. Soc. Rev.* **2006**, *35*, 583 – 592.

[13] A. D. McNaught, *Compendium of chemical terminology*, *Vol. 1669*, Blackwell Science, Oxford, **1997**.

Received: May 9, 2016
Published online: August 4, 2016

